Low-Complexity Polar-Coded Iterative OTFS Receiver

Huihou Zhang, Lianyou Jing, *Member, IEEE*, Nan Zhao, *Senior Member, IEEE*, Chengbing He, *Senior Member, IEEE*, and Yonghui Li, *Fellow, IEEE*

***Abstract*— The orthogonal time-frequency space (OTFS) modulation has gained significant attention, due to its robust performance in high-speed mobile environment. In this correspondence, we develop a novel approach wherein delay-Doppler grid symbols into vectors are organized according to their Doppler index for OTFS. A novel detection algorithm is proposed in the Doppler transform domain, which offers lower complexity and better bit error rate (BER) performance compared to existing OTFS detection algorithms. In addition, considering the superior performance of short-block polar codes, we integrate them to further enhance the performance. Simulation results validate the performance advantages of the proposed algorithm over existing benchmarks in terms of BER for OTFS. Specifically, BER performance can be improved by at least 1 dB.**

***Index Terms*— OTFS, detection, low complexity, polar codes.**

I. Introduction

THE growing demand for high-speed mobile communications, particularly in scenarios like high-speed trains (up to 500 km/h) and airplanes (up to 1,000 km/h), presents a critical challenge for reliable transmission. Orthogonal time-frequency space (OTFS) modulation has emerged as an effective solution to enhance communication reliability [1]. Unlike Orthogonal Frequency Division Multiplexing (OFDM), OTFS operates in the delay-Doppler (DD) domain, leveraging the characteristic that the Doppler shifts of time-varying channels remain nearly constant.This allows the transformation of a time-variant channels into time-independent channels in the DD domain, which also helps to simplify the complexity of channel estimation [2].

However, despite of its advantages over OFDM, OTFS has higher complexity. For instance, the message passing (MP) algorithm is a nonlinear iterative detection for OTFS, and its complexity depends on the sparsity of channels [3]. To reduce the complexity of OTFS detection, several works have focused on the linear detection. In [4], Cheng et al. utilized the double block cyclic characteristic of the channel matrix and employed the two-dimensional fast Fourier transform to implement the zero-forcing (ZF) and minimum mean square error (MMSE) equalization. Li et al. in [5] introduced a novel MMSE detection algorithm based on successive interference cancellation. In [6], Thaj and Viterbo proposed a maximum ratio combining (MRC) algorithm based on decision feedback equalization (DFE) for the zero padding OTFS.

As a fundamental technique within the domain of physical layer, channel coding plays a critical role in improving the BER performance. Integrating LDPC codes into OTFS has been demonstrated to improve the BER performance [7]. In [8], Tian et al. employed the nonbinary LDPC codes, thereby realizing an augmented coding gain within the framework of OTFS. As an emerging coding scheme, polar codes have received extensive attention in recent years [9]. Compared with LDPC, polar codes exhibit superior performance at short block lengths [10]. However, the research of polar codes has been focused on the OFDM systems, while applications of polar codes for OTFS remain limited. A notable attempt by [11] has integrated polar codes with OTFS, but further research is required to fully harness their potential in this domain.

Inspired by existing works, we propose a novel low-complexity OTFS detection algorithm. We first group the delay-Doppler grid symbols into vectors according to their Doppler index and reformulate the input-output relationship between the transmitted and received frames. Then, we apply the ZF equalization in the Doppler-transform domain for each Doppler index and combine all Doppler indices. To further improve the performance, we employ the polar codes to encode OTFS due to its superior performance at short block lengths, and develop an iterative detection algorithm for the polar codes within the proposed OTFS framework.

II. OTFS System Model

In this section, we first introduce the polar-coded OTFS transmitter, and then present the receiver in OTFS.

A. Transmitter

At the transmitter, we consider the $M \times N$ delay-Doppler grid. In the view of excellent performance of polar codes in short codes, we choose to encode each column in the grid independently to ensure that the length of each column after encoding and modulation is M. In this context, the information bits are divided into N groups, i.e., $\{\mathbf{u}_n\}_{n=0}^{N-1}$. The length of

Received 21 October 2024; accepted 5 November 2024. Date of publication 8 November 2024; date of current version 10 January 2025. This work was supported by the National Natural Science Foundation of China(62471397), the Stable Supporting Fund of Acoustic Science and Technology Laboratory (JCKYS2024604SSJS010). The associate editor coordinating the review of this letter and approving it for publication was F. Ercan. *(Corresponding author: Lianyou Jing.)*

Huihou Zhang and Nan Zhao are with the School of Information and Communication Engineering, Dalian University of Technology, Dalian, Liaoning 116024, China (e-mail: 125041897@mail.dlut.edu.cn; zhaonan@dlut.edu.cn).

Lianyou Jing is with the Ocean Institute, Northwestern Polytechnical University, Taicang, Jiangsu 215400, China (e-mail: lyjing@nwpu.edu.cn).

Chengbing He is with the School of Marine Science and Technology, Northwestern Polytechnical University, Xi'an, Shaanxi 710072, China (e-mail: hcb@nwpu.edu.cn).

Yonghui Li is with the School of Electrical and Information Engineering, The University of Sydney, Sydney, NSW 2006, Australia (e-mail: yonghui.li@sydney.edu.au).

Digital Object Identifier 10.1109/LCOMM.2024.3493962

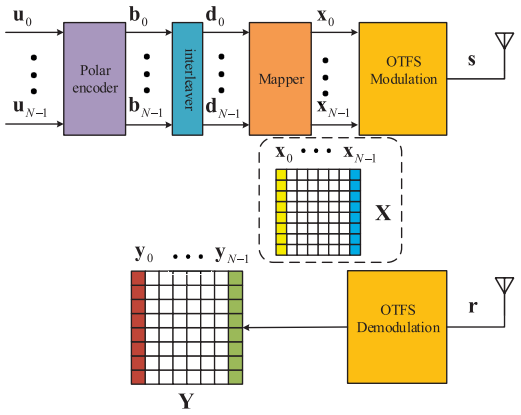

Fig. 1. The polar-coded OTFS system.

each group of information bits is M_a. Thus, there are M_aN bits for a single OTFS frame.

Then, we perform the polar coding for each group of bits $\mathbf{u}_n$. To realize channel polarization and estimate channel reliability, the Gaussian Approximation (GA) method is employed, which reduces computational complexity by approximating the probability density function of the log-likelihood ratios (LLR) during the density evolution process as a Gaussian distribution [12]. After that, the channels are sorted according to the reliability, the channel with the highest reliability (i.e., the lowest error probability) is utilized to transmit $\mathbf{u}_n$, and the remaining channels are leveraged to transmit the frozen bits.

When $\mathbf{u}_n$ is mapped to the selected reliable channel, we can get source bit vector $\mathbf{g}_n$ with the length $M_b = M_a/R$, where R is the code rate. Furthermore, the generator matrix $\mathbf{G}_{M_b} \in \mathbb{C}^{M_b \times M_b}$ of polar encoding can be defined as [13]

$$\mathbf{G}_{M_b} = \mathbf{B}_{M_b}\mathbf{F}^{\otimes b}, b = \log_2(M_b), \tag{1}$$

where $\mathbf{F}^{\otimes b}$ is the b-fold Kronecker product of $\mathbf{F} = \begin{bmatrix} 1 & 0 \\ 1 & 1 \end{bmatrix}$. $\mathbf{B}_{M_b} \in \mathbb{C}^{M_b \times M_b}$ is a permutation matrix to complete the bit reverse reordering operation, which can be obtained by the recursive formula as

$$\mathbf{B}_{M_b} = \mathbf{R}_{M_b}\left(\mathbf{I}_2 \otimes \mathbf{B}_{M_b/2}\right), \mathbf{B}_2 = \mathbf{I}_2, \tag{2}$$

where $\mathbf{R}_{M_b} \in \mathbb{C}^{M_b \times M_b}$ is a permutation matrix to separate the odd-order elements and even-order elements from the input sequence. After constructing the generating matrix $\mathbf{G}_{M_b}$, $\mathbf{g}_n$ can be encoded to obtain $\mathbf{b}_n \in \mathbb{C}^{M_b \times 1}$ as

$$\mathbf{b}_n = \mathbf{g}_n\mathbf{G}_{M_b}. \tag{3}$$

After the polar encoding, we interleave $\mathbf{b}_n$ to obtain $\mathbf{d}_n \in \mathbb{C}^{M_b \times 1}$, and map $\mathbf{d}_n$ to the column vector $\mathbf{x}_n = [\mathbf{X}(0,n), \mathbf{X}(1,n), \ldots, \mathbf{X}(M-1,n)]^{\mathrm{T}} \in \mathbb{C}^{M \times 1}$ in the delay-Doppler domain matrix $\mathbf{X} \in \mathbb{C}^{M \times N}$ by the $\mathcal{Q}$-QAM modulation, where $M = M_b/\log_2\mathcal{Q}$. Fig. 1 shows the polar-coded OTFS system.

After the QAM modulation, the signal matrix $\mathbf{X}_{\mathrm{tf}}$ can be obtained in the time-frequency domain by the inverse symplectic Fourier transform as

$$\mathbf{X}_{\mathrm{tf}} = \mathbf{F}_M\mathbf{X}\mathbf{F}_N^{\dagger}, \tag{4}$$

where $\mathbf{F}_N$ and $\mathbf{F}_N^{\dagger}$ represent the normalized N-point DFT matrix and its conjugate transpose. Then the symbols in the time-frequency domain are converted to the time domain as

$$\mathbf{s} = \mathrm{vec}\left(\mathbf{G}_{\mathrm{tx}}\left(\mathbf{F}_M^{\dagger}\mathbf{X}_{\mathrm{tf}}\right)\right) = \mathrm{vec}\left(\mathbf{G}_{\mathbf{tx}}\left(\mathbf{X}\mathbf{F}_N^{\dagger}\right)\right), \tag{5}$$

where the matrix $\mathbf{G}_{\mathrm{tx}}$ is the pulse shaping filter at the transmitter. The operator $\mathrm{vec}(\cdot)$ denotes the transformation of a matrix into its column vector form, and $\mathrm{vec}_{M,N}^{-1}(\cdot)$ represents the process of folding a vector into a $M \times N$ matrix. In this letter, we only consider the case of transmitting a rectangular pulse, i.e., $\mathbf{G}_{\mathrm{tx}} = \mathbf{I}_M$, and have

$$\mathbf{s} = \mathrm{vec}\left(\mathbf{X}\mathbf{F}_N^{\dagger}\right). \tag{6}$$

Subsequently, a cyclic prefix (CP) is added to the front of $\mathbf{s}$ and transmitted over a time-varying channel.

B. Receiver

After removing the CP, we first transform the time-domain received channel vector $\mathbf{r} \in \mathbb{C}^{MN \times 1}$ into a matrix $\mathbf{R} \in \mathbb{C}^{M \times N}$, and then perform the Wigner transform on the received signal to obtain the time-frequency domain signal as

$$\mathbf{Y}_{\mathrm{tf}} = \mathbf{F}_M\mathbf{G}_{\mathrm{rx}}\mathbf{R} = \mathbf{F}_M\mathbf{G}_{\mathrm{rx}}\mathrm{vec}_{M,N}^{-1}(\mathbf{r}). \tag{7}$$

In this letter, we only consider the case that the received pulse is rectangular, i.e., $\mathbf{G}_{\mathrm{rx}} = \mathbf{I}_M$. Then, by the symplectic Fourier transform of the received signal $\mathbf{Y}_{\mathrm{tf}}$ in the time-frequency domain, the signal $\mathbf{Y} \in \mathbb{C}^{M \times N}$ in the delay-Doppler domain can be obtained as

$$\mathbf{Y} = \mathbf{F}_M^{\dagger}\mathbf{Y}_{\mathrm{tf}}\mathbf{F}_N = \mathrm{vec}_{M,N}^{-1}(\mathbf{r})\mathbf{F}_N. \tag{8}$$

After obtaining the received signal matrix $\mathbf{Y}$, the transmitted signal vector is estimated using the Doppler-transform domain equalization detector, and then decoded to obtain the corresponding information bits. The detailed procedure of the proposed detector is presented in the next section.

III. Proposed Low Complexity Detector

In this section, we propose the iterative Doppler-transform domain equalization detector for polar-coded OTFS schemes and analyze its complexity.

A. Iterative Delay-Transform Domain Equalization Detector

The input-output relationship of OTFS in the delay-Doppler domain can be given as [14]

$$\mathbf{y} = \mathbf{H}\mathbf{x} + \mathbf{w}, \tag{9}$$

where $\mathbf{x} = \mathrm{vec}(\mathbf{X}), \mathbf{y} = \mathrm{vec}(\mathbf{Y}) \in \mathbb{C}^{MN \times 1}$ are the column vectorized matrices of $\mathbf{X}$ and $\mathbf{Y}$. $\mathbf{w}$ is the additive white Gaussian noise (AWGN) with variance σ^2, and $\mathbf{H} \in \mathbb{C}^{MN \times MN}$ is the channel matrix between transmitted and received symbol vectors, which can be represented as

$$\mathbf{H} = \sum_{i=1}^{P} h_i\left(\mathbf{F}_N \otimes \mathbf{I}_M\right)\mathbf{\Pi}_{MN}^{l_i}\mathbf{\Delta}^{k_i}\left(\mathbf{F}_N^{\dagger} \otimes \mathbf{I}_M\right), \tag{10}$$

where P represents the number of multipaths, while h_i, l_i and k_i denote the complex gain, normalized delay, and normalized Doppler shift of the i-th path in the channel, respectively. $\mathbf{\Pi}_{MN} \in \mathbb{C}^{MN\times MN}$ is the permutation matrix, $\mathbf{\Delta} = \text{diag}\left[e^{\frac{j2\pi\cdot 0}{MN}}, e^{\frac{j2\pi\cdot 1}{MN}}, \ldots, e^{\frac{j2\pi\cdot(MN-1)}{MN}}\right] \in \mathbb{C}^{MN\times MN}$ is the diagonal matrix.

According to (10), $\mathbf{H}$ can be rewritten as

$$\mathbf{H} = \sum_{i=1}^{P} h_i \left(\mathbf{F}_N \otimes \mathbf{I}_M\right) \mathbf{\Pi}_{MN}^{l_i} \left(\mathbf{F}_N^{\dagger} \otimes \mathbf{I}_M\right) \cdot \left(\mathbf{F}_N \otimes \mathbf{I}_M\right) \mathbf{\Delta}^{k_i} \left(\mathbf{F}_N^{\dagger} \otimes \mathbf{I}_M\right). \tag{11}$$

Subsequently, $\mathbf{H}$ can be decomposed as follows

$$\mathbf{H} = \sum_{i=1}^{P} \mathbf{V}_i \mathbf{D}_i, \tag{12}$$

where

$$\mathbf{V}_i = h_i \left(\mathbf{F}_N \otimes \mathbf{I}_M\right) \mathbf{\Pi}_{MN}^{l_i} \left(\mathbf{F}_N^{\dagger} \otimes \mathbf{I}_M\right), \tag{13}$$

$$\mathbf{D}_i = \left(\mathbf{F}_N \otimes \mathbf{I}_M\right) \mathbf{\Delta}^{k_i} \left(\mathbf{F}_N^{\dagger} \otimes \mathbf{I}_M\right). \tag{14}$$

Note that $\mathbf{V}_i$ is a block diagonal matrix, which can be represented by

$$\mathbf{V}_i = \text{diag}\left[\mathbf{V}_{i,0}, \mathbf{V}_{i,1}, \ldots, \mathbf{V}_{i,n}, \ldots, \mathbf{V}_{i,N-1}\right]. \tag{15}$$

Since $\mathbf{\Delta}$ is a diagonal matrix, $\mathbf{D}_i$ in (14) is block diagonal matrix, which can be simplified as

$$\begin{aligned}\mathbf{D}_i &= \mathbf{\Pi}_N^{k_i} \otimes \mathbf{\Lambda}_M^{-k_i} \\ &= \text{diag}\left[\mathbf{\Lambda}_M^{-k_i}, \mathbf{\Lambda}_M^{-k_i}, \ldots, \mathbf{\Lambda}_M^{-k_i}\right] \mathbf{\Pi}_{MN}^{Mk_i},\end{aligned} \tag{16}$$

where $\mathbf{\Lambda}_M = \text{diag}\left[e^{\frac{j2\pi\cdot 0}{MN}}, e^{\frac{j2\pi\cdot 1}{MN}}, \ldots, e^{\frac{j2\pi\cdot(M-1)}{MN}}\right]$.

Finally, according to (15) and (16), the channel matrix $\mathbf{H}$ can be rewritten as

$$\mathbf{H} = \sum_{i=1}^{P} \text{diag}\left[\mathbf{V}_{i,0}\mathbf{\Lambda}_M^{-k_i}, \ldots, \mathbf{V}_{i,N-1}\mathbf{\Lambda}_M^{-k_i}\right] \mathbf{\Pi}_{MN}^{Mk_i}. \tag{17}$$

Consequently, we analyze the relationships between input and output symbol vectors after block-wise processing. In this context, $\mathbf{x}_n, \mathbf{y}_n, \mathbf{w}_n \in \mathbb{C}^{M\times 1}$ are defined as the block vectors of $\mathbf{x} = \left[\mathbf{x}_0^{\mathrm{T}}, \mathbf{x}_1^{\mathrm{T}}, \ldots, \mathbf{x}_{N-1}^{\mathrm{T}}\right]^{\mathrm{T}}$, $\mathbf{y} = \left[\mathbf{y}_0^{\mathrm{T}}, \mathbf{y}_1^{\mathrm{T}}, \ldots, \mathbf{y}_{N-1}^{\mathrm{T}}\right]^{\mathrm{T}}$, $\mathbf{w} = \left[\mathbf{w}_0^{\mathrm{T}}, \mathbf{w}_1^{\mathrm{T}}, \ldots, \mathbf{w}_{N-1}^{\mathrm{T}}\right]^{\mathrm{T}}$, respectively.

By combining the permutation matrix $\mathbf{\Pi}_{MN}^{Mk_i}$ and the vector $\mathbf{x}$, we get

$$\mathbf{y}_n = \sum_{i=1}^{P} \mathbf{V}_{i,n}\mathbf{\Lambda}_M^{-k_i}\mathbf{x}_{[n-k_i]_N} + \mathbf{w}_n. \tag{18}$$

Note that (18) can be further rewritten as

$$\begin{aligned}\mathbf{y}_{[n+k_i]_N} &= \mathbf{V}_{i,[n+k_i]_N}\mathbf{\Lambda}_M^{-k_i}\mathbf{x}_n + \sum_{i'\neq i, i'\in P} \mathbf{V}_{i',[n+k_{i'}]_N} \cdot \mathbf{\Lambda}_M^{-k_{i'}}\mathbf{x}_{[n+k_i-k_{i'}]_N} + \mathbf{w}_{[n+k_i]_N} \\ &= \mathbf{V}_{i,[n+k_i]_N}\mathbf{\Lambda}_M^{-k_i}\mathbf{x}_n + \xi_n^i + \mathbf{w}_{[n+k_i]_N},\end{aligned} \tag{19}$$

where ξ_n^i is the interference from other Doppler indices as

$$\xi_n^i = \sum_{i'\neq i, i'\in P} \mathbf{V}_{i',[n+k_{i'}]_N}\mathbf{\Lambda}_M^{-k_{i'}}\mathbf{x}_{[n+k_i-k_{i'}]_N}. \tag{20}$$

The block matrix $\mathbf{V}_{i,n} \in \mathbb{C}^{M\times M}$ can be decomposed into the following form as [15]

$$\mathbf{V}_{i,n} = \mathbf{\Lambda}_M^{n\,\dagger}\mathbf{F}_M^{\dagger}\mathbf{T}_{i,n}\mathbf{F}_M\mathbf{\Lambda}_M^n, \tag{21}$$

where $\mathbf{T}_{i,n}$ is the diagonal matrix generated by the channel gain $H_{i,q} = \sum_{l\in\mathcal{L}} h_i e^{\frac{-j2\pi\cdot ql}{MN}}$ $(q = 0, \ldots, MN-1)$ under different paths as

$$\mathbf{T}_{i,n} = \text{diag}\left[H_{i,n}, H_{i,n+N}, \ldots, H_{i,n+(M-1)N}\right]. \tag{22}$$

Thus, (19) can be rewritten as

$$\mathbf{y}_{[n+k_i]_N} = \left(\mathbf{\Lambda}_M^{[n+k_i]_N}\right)^{\dagger}\mathbf{F}_M^{\dagger}\mathbf{T}_{i,[n+k_i]_N}\mathbf{F}_M\mathbf{\Lambda}_M^n\mathbf{x}_n + \xi_n^i + \mathbf{w}_{[n+k_i]_N}. \tag{23}$$

By multiplying $\mathbf{F}_M\mathbf{\Lambda}_M^{[n+k_i]_N}$ on both sides of (23), we can obtain

$$\begin{aligned}\bar{\mathbf{y}}_{[n+k_i]_N} &= \mathbf{F}_M\mathbf{\Lambda}_M^{[n+k_i]_N}\mathbf{y}_{[n+k_i]_N} \\ &= \mathbf{T}_{i,[n+k_i]_N}\mathbf{F}_M\mathbf{\Lambda}_M^n\mathbf{x}_n + \mathbf{F}_M\mathbf{\Lambda}_M^{[n+k_i]_N}\xi_n^i + \mathbf{F}_M\mathbf{\Lambda}_M^{[n+k_i]_N}\mathbf{w}_{[n+k_i]_N} \\ &= \mathbf{T}_{i,[n+k_i]_N}\bar{\mathbf{x}}_n + \bar{\xi}_n^i + \bar{\mathbf{w}}_{[n+k_i]_N},\end{aligned} \tag{24}$$

where $\bar{\mathbf{x}}_n = \mathbf{F}_M\mathbf{\Lambda}_M^n\mathbf{x}_n$ and $\bar{\mathbf{w}}_{[n+k_i]_N} = \mathbf{F}_M\mathbf{\Lambda}_M^{[n+k_i]_N}\mathbf{w}_{[n+k_i]_N}$.

Since $\bar{\mathbf{x}}_n$ and $\bar{\mathbf{y}}_n$ are obtained by applying FFT on the DD domain vector, we call them in the *Doppler-transform domain*. $\mathbf{T}_{i,[n+k_i]_N}$ is a diagonal matrix. According to (24), the ZF equalization can be performed in the Doppler-transform domain after eliminating the interference of other Doppler indices as

$$\hat{\bar{\mathbf{x}}}_n^i(m) = \left(\bar{\mathbf{y}}_{[n+k_i]_N}(m) - \bar{\xi}_n^i(m)\right) / \left(H_{i,n+(m-1)N}\right). \tag{25}$$

Then, the estimates under different Doppler indices can be combined as

$$\hat{\bar{\mathbf{x}}}_n = \sum_{i=1}^{P} \frac{h_i^2 \cdot \hat{\bar{\mathbf{x}}}_n^i}{h_{si}}, \tag{26}$$

where $h_{si} = \sum_{i=1}^{P} h_i^2$ is the gain corresponding to each path in the channel.

Finally, the estimated value $\tilde{\mathbf{x}}_n$ is reconverted in the Doppler-transform domain to the DD domain as

$$\mathbf{c}_n = (\mathbf{\Lambda}_M^n)^{\dagger}\mathbf{F}_M^{\dagger}\hat{\bar{\mathbf{x}}}_n. \tag{27}$$

To achieve efficient polar code decoding, the CRC-aided successive cancellation list (CA-SCL) decoding algorithm with the size of list L is employed [16]. For simplicity, we denote the estimated value of the source bit vector $\hat{\mathbf{g}}_n$ as $\hat{\mathbf{g}}$, and the estimated vector $\mathbf{c}_n$ as $\mathbf{c}$.

The decoding algorithm for the vector can be represented as search over a binary tree of depth M_b. To select the optimal set of L paths, it is necessary to define a likelihood metric for each path, enabling comparison and subsequent filtering. The metric for the l_i-th $(l_i = 0, \ldots, L)$ path at the m_b-th $(m_b = 0, \ldots, M_b)$ level of the code tree can be expressed as

$$\text{PM}_{l_i}^{(m_b)} = \sum_{j=1}^{m_b} \ln\left(1 + e^{-(1-2\hat{\mathbf{g}}_j[l_i])\Gamma_{j,l_i}}\right), \tag{28}$$

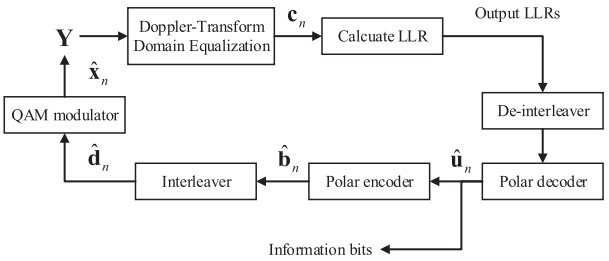

Fig. 2. Doppler-transform domain equalization detector.

where $\mathbf{g}_j[l_i]$ denotes the estimated value of the l_i-th path from the j-th layer, while Γ_{m_b,l_i} is the LLR of $\mathbf{g}_{m_b}[l_i]$, which can be represented by

$$\Gamma_{m_b,l_i} = \ln \frac{W_{M_b}^{(m_b)}\left(\mathbf{c}, \hat{\mathbf{g}}_1^{m_b-1}[l_i] \middle| \hat{\mathbf{g}}(m_b)=0\right)}{W_{M_b}^{(m_b)}\left(\mathbf{c}, \hat{\mathbf{g}}_1^{m_b-1}[l_i] \middle| \hat{\mathbf{g}}(m_b)=1\right)}, \tag{29}$$

where W_{M_b} denotes the channel shift probability and $\mathbf{g}_1^{m_b-1}[l_i]$ denotes the estimated value of the layers 1 through m_b on the l_i-th path. Considering the adoption of QAM modulation, Γ_{m_b,l_i} need to be decomposed into Γ_{m,b_0,l_i} and Γ_{m,b_1,l_i} for separate calculations (taking 4-QAM as an example):

$$\Gamma_{m,b_0,l_i} = \ln \frac{p(\mathbf{c}(m)|b_0=0)}{p(\mathbf{c}(m)|b_0=1)} = \frac{2\cdot re(\mathbf{c}(m))}{\sigma^2}, \tag{30}$$

$$\Gamma_{m,b_1,l_i} = \ln \frac{p(\mathbf{c}(m)|b_1=0)}{p(\mathbf{c}(m)|b_1=1)} = \frac{2\cdot im(\mathbf{c}(m))}{\sigma^2}, \tag{31}$$

where b_0 and b_1 are the symbols corresponding to the real and imaginary parts of $\mathbf{c}$, respectively. As the number of decoding layers increases, the path metric can be updated by

$$\mathrm{PM}_{l_i}^{(m_b)} = \mathrm{PM}_{l_i}^{(m_b-1)} + \ln\left(e^{-\left(1-2\hat{\mathbf{g}}_{m_b}[l_i]\right)\Gamma_{m_b,l_i}}\right). \tag{32}$$

After each path expansion, the L paths with the smallest metrics are selected and stored for the next iteration, continuing until the code tree reaches the M_b-th layer. The candidate paths are then sorted in ascending order by their metrics, followed by sequential CRC checks. The first path that passes the CRC check is selected as the estimated source bits $\hat{\mathbf{g}}_n$, and the information bits $\hat{\mathbf{u}}_n$ are derived based on the information bit positions.

Once the estimated $\hat{\mathbf{u}}_n$ is updated, we increase n and repeat the same to estimate all vectors. During the estimation, since the interference from other Doppler indices need to be computed, we reconstruct the estimated $\mathbf{x}_n$ used for estimating other vectors by recoding and mapping $\hat{\mathbf{u}}_n$. Fig. 2 shows the flowchart of Doppler-transform domain equalization detector.

After estimating all $\mathbf{x}_n$, we repeat the equalization until reach the maximum iterations I_{iter} or decoding without errors. The algorithm of the proposed Doppler-transform domain iterative detector is summarized in Algorithm 1.

B. Complexity Analysis

In the process of Doppler-transform domain equalization, the complexity of calculating $\hat{\hat{\mathbf{x}}}_n^i$ in each iteration is $\mathcal{O}\left(P^2M\right)$, and the complexity of combining $\hat{\hat{\mathbf{x}}}_n^i$ to obtain $\hat{\mathbf{x}}_n$ is $\mathcal{O}(PM)$. The complexity of (27) can be reduced by IFFT to $\mathcal{O}(M\log_2 M)$. Therefore, the complexity of the equalization process is $\mathcal{O}\left(I_{iter}N\left(P^2M + M\log_2 M\right)\right)$.

During the decoding process, the complexity of applying the CA-SCL decoder to each column vector is $\mathcal{O}(I_{iter}LM\log_2 M)$. Therefore, the total complexity of the decoding process is $C_{CA-SCL} = \mathcal{O}(I_{iter}LNM\log_2 M)$. In summary, the overall complexity of the iterative detection algorithm is $C_{CA-SCL} + \mathcal{O}\left(I_{iter}N\left(P^2M + M\log_2 M\right)\right)$.

Algorithm 1 Doppler-Transform Domain Iterative Detector

Input: $\mathbf{T}_{i,n}, \mathbf{\Lambda}_M, h_i, h_{si}, \mathbf{y}_n, \quad \forall n = 0,\ldots,N-1$
Initialize: $\hat{\mathbf{x}}_n = \mathbf{0}_M, \quad \forall n = 0,\ldots,N-1$
for $i_{iter} = 1{:}I_{iter}$ **do**
  for $n = 0 : N-1$ **do**
    for $i = 1 : P$ **do**
      Update $\hat{\hat{\mathbf{x}}}_n^i$ by using $\bar{\mathbf{y}}_{[n+k_i]_N}, \bar{\xi}_n^i$ and $\mathbf{T}_{i,[n+k_i]_N}$ based on (25)
      Combine $\hat{\hat{\mathbf{x}}}_n^i$ to obtain $\hat{\mathbf{x}}_n$ based on (26)
    end
    Transform $\hat{\mathbf{x}}_n$ to $\mathbf{c}_n$ based on (27)
    Compute the LLR value $\Gamma_{m,b_{0,1},l_i}$ of $\mathbf{c}_n$ based on (30) and (31)
    De-interleave LLR and utilize the CA-SCL decoding to obtain $\hat{\mathbf{u}}_n$
    Re-coding, interleaving and mapping $\hat{\mathbf{u}}_n$ to obtain $\hat{\mathbf{x}}_n$
  end
end

IV. Simulation Results

In this section, the performance of the proposed scheme is verified via simulations. The subcarrier spacing Δf is 15 kHz and the carrier frequency is 4GHz. We adopt 4-QAM modulation. The channel path gain h_i, and delay τ_i of each path generated according to the standard extended vehicle A model. The Doppler frequency shift for each path is calculated as $\nu_i = \nu_{\max}\cos(\theta_i)$, where ν_{max} represents the maximum Doppler frequency shift and $\theta_i \sim \mathrm{U}[-\pi,\pi]$. The user speed is set to 500 kmph, corresponding to $\nu_{max} = 1853$ kHz.

First, the performance of the proposed detection algorithms is compared with MP detection [3] and MRC detection [6] for an uncoded system. Here, we set $M = 128$, $N = 64$, the number of iterations of the proposed detection algorithms and MRC detection $I_{iter} = 4$, and the number of iterations of MP detection $N_{iter} = 10$. In Fig. 3(a), the BER performance of each algorithm is presented under different number of multipaths, where the signal-to-noise ratio (SNR) is 10 dB. The BER curves demonstrate the superiority of the proposed algorithm. The complexity of different detection algorithms is compared in Table I, while Fig. 3(b) illustrates the number of complex multiplications (CMs) performed by each algorithm under varying number of multipaths. Specifically, when the number of multipaths $P = 9$, the proposed algorithm uses only approximately 7.14% of the CMs required by the MP detection

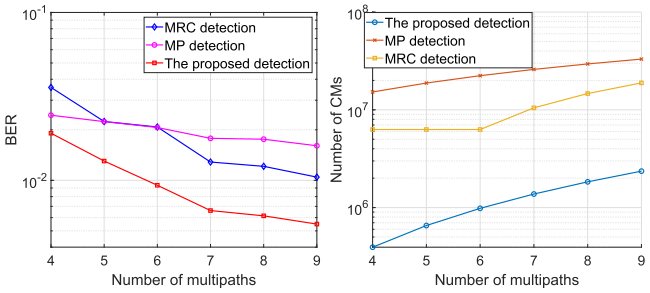

(a) BER Performance (b) Number of CMs

Fig. 3. Comparison of BER performance and CMs under different number of multipaths.

TABLE I
COMPLEXITY OF DETECTION ALGORITHMS

Detection Algorithm	Complexity
MRC detection	$\mathcal{O}\left(M\left(\lvert\mathcal{L}\rvert N^3 + I_{iter}\lvert\mathcal{L}\rvert^2 N^2\right)\right)$
MP detection	$\mathcal{O}\left(N_{iter}NMSQ\right)$
Doppler-transform domain equalization	$\mathcal{O}\left(I_{iter}N\left(P^2M + M\log_2 M\right)\right)$

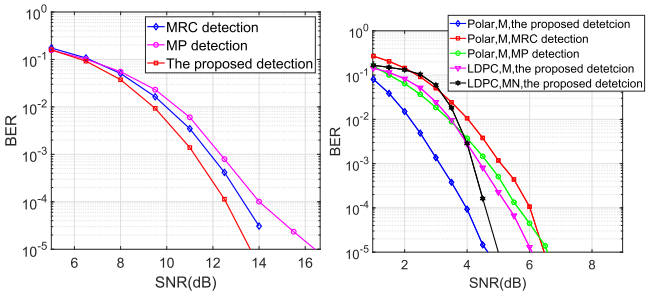

(a) Uncoded system (b) Coded system

Fig. 4. The BER performance comparison of different detection algorithms.

and 12.5% of the CMs required by the MRC detection. Therefore, it is obvious that the complexity of Doppler transform domain equalization is lower than that of MP detection and MRC detection.

Fig. 4(a) presents the BER comparison of the three detection algorithms. Compared to MRC and MP, the proposed detection method achieves approximately 1 dB and 2 dB gain at the BER of 1e-4, respectively. This demonstrates the superior BER performance of the proposed algorithm over MRC and MP detection.

Then, the performance of the proposed scheme is shown for the coded system, compared with LDPC code. Two benchmarks are considered. In the first benchmark, the code length matches that of the vector. In the second benchmark, the code length equals the length of the entire information bit. The code rate R is set to 0.5. In order to avoid excessive coding gain, we set $M = 32$ and $N = 16$, and the list length of the CA-SCL decoder is set to 16. The comparison results is shown in Fig. 4(b), colorblackcompared to LDPC code of lengths M and MN, polar code provides encoding gains of approximately 2 dB and 1 dB at the BER of 10^{-4}, respectively, demonstrating the superiority of polar code at short block lengths. Moreover, under the same polar code encoding conditions, the proposed detection also significantly outperforms MP detection and MRC detection.

V. CONCLUSION

In this correspondence, we constructed the input-output relationship of the signal vectors according to the Doppler index, and proposed a Doppler-transform domain equalization algorithm. The algorithm has better BER performance and lower complexity than the original MRC and MP algorithms. In addition, considering the performance advantages of polar code in short codes, we added the encoding and decoding process of polar codes to the OTFS system to obtain better BER performance. Simulation results showed the superiority of the algorithm in BER performance and complexity.

REFERENCES

[1] R. Hadani et al., "Orthogonal time frequency space modulation," in *Proc. IEEE Wireless Commun. Netw. Conf. (WCNC)*, San Francisco, CA, USA, Mar. 2017, pp. 1–6.

[2] Y. Liu, S. Zhang, F. Gao, J. Ma, and X. Wang, "Uplink-aided high mobility downlink channel estimation over massive MIMO-OTFS system," *IEEE J. Sel. Areas Commun.*, vol. 38, no. 9, pp. 1994–2009, Sep. 2020.

[3] P. Raviteja, K. T. Phan, Y. Hong, and E. Viterbo, "Interference cancellation and iterative detection for orthogonal time frequency space modulation," *IEEE Trans. Wireless Commun.*, vol. 17, no. 10, pp. 6501–6515, Oct. 2018.

[4] J. Cheng, H. Gao, W. Xu, Z. Bie, and Y. Lu, "Low-complexity linear equalizers for OTFS exploiting two-dimensional fast Fourier transform," 2019, *arXiv:1909.00524*.

[5] Q. Li, J. Yuan, M. Qiu, S. Li, and Y. Xie, "Low complexity turbo SIC-MMSE detection for orthogonal time frequency space modulation," *IEEE Trans. Commun.*, vol. 72, no. 6, pp. 3169–3183, Jun. 2024.

[6] T. Thaj and E. Viterbo, "Low complexity iterative rake decision feedback equalizer for zero-padded OTFS systems," *IEEE Trans. Veh. Technol.*, vol. 69, no. 12, pp. 15606–15622, Dec. 2020.

[7] P. Priya, Y. Hong, and E. Viterbo, "Oversampled receiver for coded OTFS with different D/A reconstruction filters," *IEEE Wireless Commun. Lett.*, vol. 13, no. 9, pp. 2327–2331, Sep. 2024.

[8] H. Tian, D. Zhao, and H. Jia, "Research on nonbinary LDPC-OTFS scheme in high mobile communication scenarios," in *Proc. Int. Conf. Eng. Emerg. Technol. (ICEET)*, Istanbul, Turkey, Oct. 2021, pp. 1–6.

[9] F. Ercan, C. Condo, and W. J. Gross, "Improved bit-flipping algorithm for successive cancellation decoding of polar codes," *IEEE Trans. Commun.*, vol. 67, no. 1, pp. 61–72, Jan. 2019.

[10] I. Tal and A. Vardy, "List decoding of polar codes," *IEEE Trans. Inf. Theory*, vol. 61, no. 5, pp. 2213–2226, May 2015.

[11] Z. Liu, J. Lei, and B. Shu, "Research on polar-OTFS technology in high-speed mobile communication scenarios," in *Proc. 13th Int. Conf. Commun., Circuits Syst. (ICCCAS)*, Xiamen, China, May 2024, pp. 244–249.

[12] P. Trifonov, "Efficient design and decoding of polar codes," *IEEE Trans. Commun.*, vol. 60, no. 11, pp. 3221–3227, Nov. 2012.

[13] E. Arikan, "Channel polarization: A method for constructing capacity-achieving codes for symmetric binary-input memoryless channels," *IEEE Trans. Inf. Theory*, vol. 55, no. 7, pp. 3051–3073, Jul. 2009.

[14] P. Raviteja, Y. Hong, E. Viterbo, and E. Biglieri, "Practical pulse-shaping waveforms for reduced-cyclic-prefix OTFS," *IEEE Trans. Veh. Technol.*, vol. 68, no. 1, pp. 957–961, Jan. 2019.

[15] J. Han, L. Zhang, Q. Zhang, and G. Leus, "Low-complexity equalization of orthogonal signal-division multiplexing in doubly-selective channels," *IEEE Trans. Signal Process.*, vol. 67, no. 4, pp. 915–929, Feb. 2019.

[16] K. Niu and K. Chen, "CRC-aided decoding of polar codes," *IEEE Commun. Lett.*, vol. 16, no. 10, pp. 1668–1671, Oct. 2012.